

## Article

# Virtual Synchronous Machine Control of RES Plants in Isolated Power Systems

Jaser A. Sa'ed <sup>1</sup>, Salvatore Favuzza <sup>2,\*</sup>, Milagros Amparo Navarro Navia <sup>2</sup> and Gaetano Zizzo <sup>2,\*</sup>

<sup>1</sup> Department of Electrical and Computer Engineering, Birzeit University, Birzeit P.O. Box 14, Palestine; jsaed@birzeit.edu

<sup>2</sup> Engineering Department, University of Palermo, 90128 Palermo, Italy; milagrosamparo.navarronavia@community.unipa.it

\* Correspondence: salvatore.favuzza@unipa.it (S.F.); gaetano.zizzo@unipa.it (G.Z.)

**Abstract:** Because of the increase in renewable energy sources (RESs) share, new control strategies of isolated power systems have been developed to improve the frequency and voltage stability of inverter-interfaced RESs. A voltage source converter (VSC) with a virtual synchronous machine (VSM) is among the most promising control schemes. This paper demonstrates how VSM control of inverter-interfaced RES can be efficiently used to improve the dynamic stability in small isolated power systems. In the proposed analysis, the RESs of a Mediterranean island are assumed interfaced to the grid by VSCs with a swing controller and a vector-current controller (VCC) with two different options for the reference current (RC) to regulate the voltage at the point of common coupling (PCC) and the real power output. The system is modelled in a PSCAD environment, and the behavior of the control is tested in the case of a phase-to-phase fault. The results of the simulations for different scenarios and values for the control parameters show the effectiveness of the control in small isolated grids. Finally, the level of grid power quality is verified via harmonic analysis of the PCC voltage.

**Keywords:** renewable energy sources; virtual synchronous machine; voltage source converter; isolated power systems; power system stability



**Citation:** Sa'ed, J.A.; Favuzza, S.; Navarro Navia, M.A.; Zizzo, G. Virtual Synchronous Machine Control of RES Plants in Isolated Power Systems. *Appl. Sci.* **2022**, *12*, 5920. <https://doi.org/10.3390/app12125920>

Academic Editors: Enrico Cagno, Mohsen Soltani, Edris Pouresmaeil and Pooya Davari

Received: 12 April 2022

Accepted: 8 June 2022

Published: 10 June 2022

**Publisher's Note:** MDPI stays neutral with regard to jurisdictional claims in published maps and institutional affiliations.



**Copyright:** © 2022 by the authors. Licensee MDPI, Basel, Switzerland. This article is an open access article distributed under the terms and conditions of the Creative Commons Attribution (CC BY) license (<https://creativecommons.org/licenses/by/4.0/>).

## 1. Introduction

### 1.1. Problem Statement

Worldwide, the higher cost of electricity from diesel and the targets for reducing greenhouse gas emissions have led to incentivize using renewable energy sources (RES) on small islands not supplied by the main transmission grid [1,2]. To achieve the same level of performance as traditional synchronous generators (SG), grid control must be substantially modified to accommodate this transformation of the small island generation system [3,4].

With recent advancements in the development of virtual synchronous machine (VSM) technologies, VSM has gained prominence in isolated power systems because of its characteristics of improving performance, flexibility, efficiency, stability, and reliability [2–6].

Nevertheless, voltage source converters (VSC) with VSM must be suitably controlled to avoid this, in the presence of short-circuits, while keeping the power system stable, as the electronic devices of the converter are subjected to currents capable of damaging them. In this context, one of the most dangerous events for VSCs is a phase-to-phase fault, as it produces to short-circuit currents that can rise to almost the 87% of the three-phase short-circuit current at the point of common coupling (PCC).

### 1.2. Literature Review

VSM topologies and schemes have attracted the interest of many researchers and several papers have been published on this promising topic [5–10]. The authors of [5] presented a literature review on VSM. In addition, this review paper introduces a detailed

discussion on modern control techniques for VSM. The authors of [6] provided a comprehensive review of the state-of-the-art VSM topologies along with a discussion on some of the challenges that will stem from the integration of RES. The authors of [7] presented an overview of different topologies to virtual inertia along with a detailed representation of the VSM structure. In addition, this review explained VSM control, which defines active and reactive power control and voltage and frequency control. U. Tamrakar et al. [8] presented a review of the virtual inertia implementation techniques. The major virtual inertia strategies are also compared and classified in this review paper. In [9], the authors discussed the use of electric vehicle chargers for providing virtual inertia while being operated as VSM. Finally, the authors of [10] proposed a VSM application for battery/supercapacitor hybrid energy storage systems to handle the stochastic power output of photovoltaic (PV), based on a new evolutionary algorithm called the backtracking search optimized algorithm for real-time tuning of the VSM parameters.

In light of the above literature review, Table 1 summarizes the key features and weaknesses of commonly used VSM control strategies.

**Table 1.** Features and concerns of different VSM control strategies (built starting from [8]).

Control Strategy	Characteristics	Issues
SG model-based	<ul style="list-style-type: none"> <li>Voltage-source implementation</li> <li>Accurate replication of SG dynamics</li> </ul>	<ul style="list-style-type: none"> <li>Numerical instability</li> </ul>
	<ul style="list-style-type: none"> <li>Frequency derivative not required</li> </ul>	<ul style="list-style-type: none"> <li>Need for a current limiter to protect the device during short-circuits</li> </ul>
	<ul style="list-style-type: none"> <li>Need for a Phase locked loop (PLL) for synchronization</li> <li>Black-start capability</li> </ul>	
Swing equation-based	<ul style="list-style-type: none"> <li>Governor is modeled as a first-order lag element</li> </ul>	<ul style="list-style-type: none"> <li>Numerical instability</li> <li>Power and frequency oscillations</li> </ul>
	<ul style="list-style-type: none"> <li>Frequency derivative not required</li> </ul>	<ul style="list-style-type: none"> <li>Need for a current limiter to protect the device during short-circuits</li> <li>Higher Rate of Change of Frequency</li> </ul>
	<ul style="list-style-type: none"> <li>Need for a PLL for synchronization</li> </ul>	
Frequency-power response-based	<ul style="list-style-type: none"> <li>Straightforward implementation</li> </ul>	<ul style="list-style-type: none"> <li>Instability due to PLL, particularly in weak grids</li> </ul>
	<ul style="list-style-type: none"> <li>Current-source implementation</li> <li>Inherent overcurrent protection</li> </ul>	<ul style="list-style-type: none"> <li>Frequency derivative required, system susceptible to noise</li> </ul>
	<ul style="list-style-type: none"> <li>Communication-less</li> </ul>	<ul style="list-style-type: none"> <li>Slow transient response</li> </ul>
Droop-based	<ul style="list-style-type: none"> <li>Very common</li> <li>Classical droop control implementation</li> </ul>	<ul style="list-style-type: none"> <li>Improper transient active power sharing</li> <li>Need for low pass filters for approximating the behavior of virtualinertia systems</li> <li>Need for specific control logics for ensuring a proper load sharing</li> </ul>

Therefore, new control strategies have been developed to improve the frequency and voltage stability of inverter-interfaced RES generators, considering both active and reactive power generation [11–15]. Among the mentioned strategies, those implemented for contrasting the natural reduction of the system inertia due to the increase in RES share [14–18] have a crucial role in the secure management of isolated power systems. In the technical literature, droop control coupled with virtual inertia is the most common grid-supporting method, but other solutions have recently been proposed.

### 1.3. Proposed Solution

VSC with VSM control is one of the most promising control schemes for imitating the dynamic response of a SG [19]. Through VSM control, it is possible to achieve a behavior

similar to that of a SG, but the converter is not guarded against overcurrent. Thus, the converter input current needs to be limited by a vector-current controller (VCC) [20,21]. In this paper, the VSM control combined with a vector-current controller is applied to the converters that are assumed to be installed in the small island of Pantelleria.

Initially, the hourly generation and demand of the island (data provided by the local utility SMEDE) are analyzed during typical winter and summer days. For both seasons, hour-by-hour power system inertia is calculated, and the most critical situations based on a reduced inertial response are identified. Subsequently, an equivalent single-bus model of the power system is created in the PSCAD environment. RES plants are represented as a unique VSC, and the conventional SGs is represented as a unique equivalent SG. The internal control model of the equivalent VSC considers the grid impedance and two different options for calculating the reference current, starting from a steady-state condition and evaluating the effects due to a phase-to-phase short-circuit simulated at the PCC. Simulations are done for different values of the control parameters, energy scenarios, system inertia and provided virtual inertia, and for two values of the short circuit ratio (SCR) to represent both a strong and a weak grid [22].

The rest of the paper is organized as follows: Section 2 presents the structure of the system under study and the mathematical representation of VSM with VCC. Section 3 reports the initial data for the simulations. Section 4 provides the results of the simulations and, finally, Section 5 reports the conclusions of the study.

## 2. Structure of the System and Proposed Converter Topology

The power system of a small island not supplied by the main transmission grid can be represented, for the aim of this study, as shown in Figure 1. The island’s generation system is characterized by a central diesel power plant, represented in Figure 1 as an equivalent SG identified as a “GRID” and connected in series to the grid impedance denoted as “Grid-Z”. All VSCs are represented by an equivalent VSC with an internal VSM-structure with VCC and an RL filter.

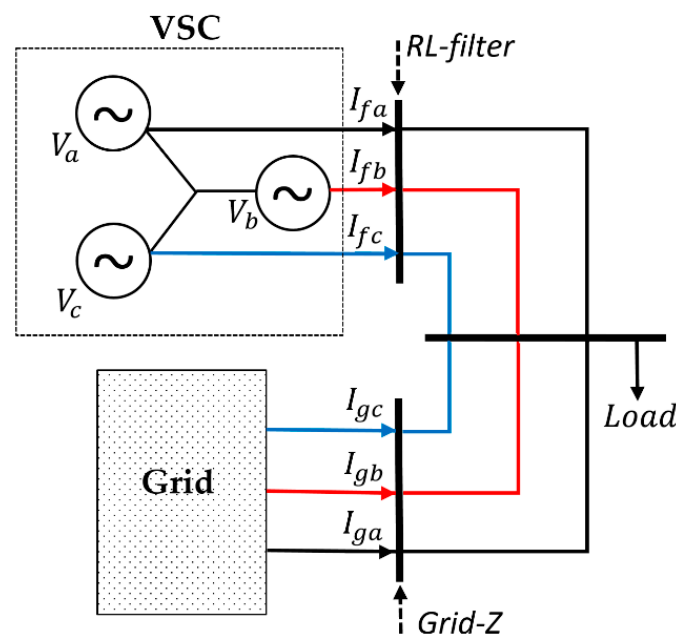


Figure 1. Equivalent model of the considered case study.

The details of the proposed topology for the VSC are described in this section, and Table 2 reports a description of all of the symbols used in the following equations.

**Table 2.** Nomenclatures employed in Equations (1)–(3).

Nomenclature	Description
$T_{vsm}$	The virtual inertia of the VSC [s]
$\omega_o$	The rated angular frequency of the system [rad/s]
$\dot{\omega}_{vsm}$	The angular frequency at the VSC [p.u.]
$P_{ref}$	The reference active power of the VSC [p.u.]
$P_{vsm}$	The actual active power output of the VSC [p.u.]
$K_{d,vsm}$	The virtual damping coefficient of the VSC
$\theta_{vsm}$	The angle position of the converter voltage concerning a reference frame synchronized with the grid and rotating at a constant frequency in steady-state [rad]
$\delta_v$	The angle between the grid voltage $V_g$ at the PCC and the output voltage of the VCS $V_{vsc}$ [rad]
$X_f$	The VSC filter reactance [p.u.]
$\theta_{vsm0}$	The steady-state virtual angle [rad]
$K_{p,vsm}$	The synchronizing torque coefficient
$\zeta$	The damping ratio
$\omega_n$	The natural frequency of the system [p.u.]

Based on the swing equation, the VSC model shows a power balance synchronization mechanism [23]:

$$2T_{vsm} \frac{d\dot{\omega}_{vsm}}{dt} = P_{ref} - P_{vsm} - K_{d,vsm} \dot{\omega}_{vsm} \quad (1)$$

$$\frac{d\theta_{vsm}}{dt} = \omega_o (\dot{\omega}_{vsm} - 1) \quad (2)$$

$$P_{vsm} = \frac{V_{vsc} V_g}{X_f} \sin(\theta_{vsm}) \quad (3)$$

Based on the aforementioned equations, a small-signal analysis of the system yields the following expression.

$$2T_{vsm} \frac{d\Delta\dot{\omega}_{vsm}}{dt} = \Delta P_{ref} - \frac{dP_{vsm}}{d\theta_{vsm}} \cdot \Delta\theta_{vsm} - K_{d,vsm} \cdot \Delta\dot{\omega}_{vsm} \quad (4)$$

$$\frac{d\Delta\theta_{vsm}}{dt} = \omega_o \cdot \Delta\dot{\omega}_{vsm} \quad (5)$$

$$\frac{dP_{vsm}}{d\theta_{vsm}} = \frac{V_{vsc} \cdot V_{PCC}}{X_f} \cdot \cos\theta_{vsm0} = K_{p,vsm} \quad (6)$$

Studying the controller response based on Equations (1) and (6) provides a relationship between the variation in output power  $\Delta P_{vsm}$  and the variation in reference power  $\Delta P_{ref}$ . Hence, the linear model of the system can be expressed as follows:

$$\frac{d}{dt} \begin{bmatrix} \Delta\dot{\omega}_{vsm} \\ \Delta\theta_{vsm} \end{bmatrix} = \begin{bmatrix} -K_{d,vsm}/2T_{vsm} & -K_{p,vsm}/2T_{vsm} \\ \omega_o & 0 \end{bmatrix} \begin{bmatrix} \Delta\dot{\omega}_{vsm} \\ \Delta\theta_{vsm} \end{bmatrix} + \begin{bmatrix} 1/2T_{vsm} \\ 0 \end{bmatrix} \Delta P_{ref} \quad (7)$$

Considering the Laplace Transform for Equations (3)–(7), the following equation is obtained:

$$\frac{\Delta P_{vsm}}{\Delta P_{ref}} = \frac{\frac{\omega_o K_{p,vsm}}{2T_{vsm}}}{s^2 + \frac{\omega_o K_{d,vsm}}{2T_{vsm}} s + \frac{\omega_o K_{p,vsm}}{2T_{vsm}}} = \frac{\omega_n^2}{(s^2 + 2\zeta\omega_n s + \omega_n^2)} \quad (8)$$

Based on the aforementioned transfer function, the active power controller poles can be determined as follows:

$$PL_{s1-2} = -\zeta \cdot \omega_n \pm \omega_n \cdot \sqrt{\zeta^2 - 1} \tag{9}$$

The VSM control guarantees the VSC has behavior similar to SG, but does not guarantee the protection of the converter from overcurrent in the presence of a short-circuit in the grid. A solution to this problem is to limit the converter current using the VCC. The VCC is one of the most common methods used for VSCs because of its simple implementation and robust performance in ideal-grid conditions. Figure 2 represents the block diagram of VSM with VCC with the reference current (RC). Seven blocks are visible:

- A measurement block at the PCC, taking the measurements of  $P_g, I_g,$  and  $V_g,$  which are the input of the RC block and the abc/dq block;
- The abc/dq and dq/abc blocks, using  $\theta_{vsm}$  for the transformations of voltages and currents;
- A damping controller denominated as DC used to improve the response in the active power of the VSC;
- A VCC used to protect the converter from overcurrent;
- An RC used to obtain the converter input of the current control and coordinate of the abc/dq and dq/abc transformations;  $P_{ref}$  and  $T_{vsm}$  are the reference variables, while  $L_f$  and  $\omega_0$  are the complementary variables.

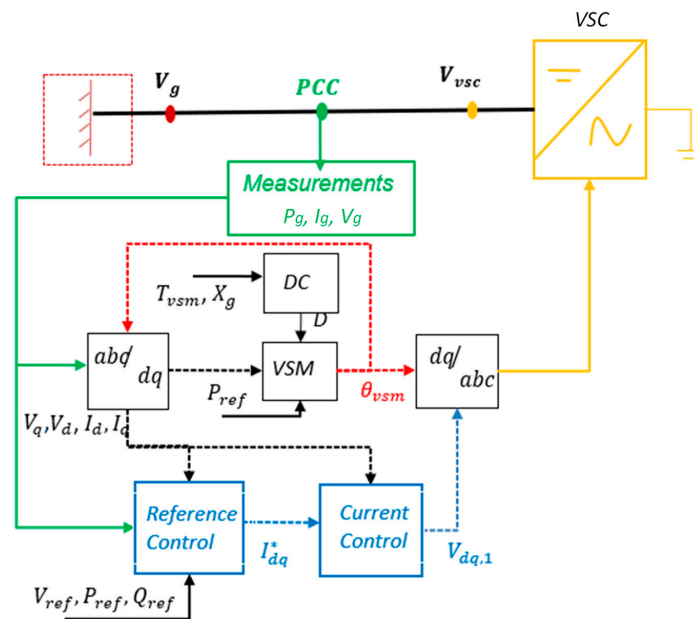


Figure 2. Block diagram of the VSM model and the main control loops.

VCC is defined by Equation (10).

$$V_{vsc}^{dq*} = V_g^{dq} + CC \cdot I_f^{dq} + PI \cdot (I_f^{dq*} - I_f^{dq}) \tag{10}$$

In this paper, the input reference current  $I_f^{dq*}$  appearing in Equation (10) is calculated using two different methods:

1. Option I (RC-1):

$$I_f^{dq*} = \left[ \frac{V_g^{dq*} - V_g^{dq} + (PI - CC) \cdot I_f^{dq}}{PI} \right] CL \tag{11}$$

In this method, by combining Equations (10) and (11), it is easy to notice that the reference current is provided to the control system in order to obtain the reference value for the VSC voltage equal to that of the grid voltage and, at the same time, to limit the current to values not dangerous for the converter, thanks to the current limiter (transfer function  $CL$ ).

2. Option II (RC-2):

$$I_f^{dq*} = \left[ \frac{V_g^{dq*} - V_g^{dq}}{\omega_o L_g} + I_f^{dq} \right] LP \cdot CL \quad (12)$$

In this method, the reference current is provided in a way that takes into account the variation in the grid voltage and the consequent variations in the grid current. In addition, in this case, the transfer function  $CL$  demonstrates the presence of a block limiting the current to values that are not dangerous for the converter.

The list of symbols employed in Equations (10)–(12) is reported in Table 3.

**Table 3.** Nomenclatures employed in Equations (10)–(13).

Nomenclature	Description
$V_{vsc}^{dq*}$	The reference signal for VSC voltage in dq coordinates
$V_g^{dq}$	The grid voltage in dq coordinates
$I_f^{dq}$	The current output of the VSC in dq coordinates
$I_f^{dq*}$	The reference current of the VSC in dq coordinates
$PI$	The transfer function of the PI controller with proportional gain $k_p = \alpha_{cc} L_t$ and integral gain $k_I = \alpha_{cc} (R_t + R_v)$
$L_t$	The sum of the VSC filter inductance $L_f$ and of the estimated grid inductance $L_g$
$R_t$	The sum of the filter resistance $R_f$ and of the estimated grid resistance $R_g$
$R_v$	The virtual resistance taking into account active damping for dealing with system parameter variations and disturbances
$\alpha_{cc}$	The desired closed-loop bandwidth of the current controller
$CC$	The transfer function of the $dq$ cross-coupling
$V_g^{dq*}$	The reference grid voltage in $dq$ coordinates
$CL$	The transfer functions of the current limiter
$LP$	The transfer function of the low-pass filter

It is worth mentioning that the  $CL$  is necessary for blocking the overcurrents during the transients, and  $LP$  is required for avoiding spiky transients and miscalculations before sending the calculated references to the current controller.

### 3. Case Study

The case study considers the 10 kV isolated power system of the island of Pantelleria in the case of the high share of RES generation. The current central power plant of the island consists of eight SGs for a total rated power of 24.5 MVA. The detailed specifications for this system are described and documented in [24,25]. The system is modelled as in Figure 1 using the control topology in Figure 2.

Based on the data provided by the local utility and considering a renewable energy mix of 1 MW photovoltaic and 1 MW wind power, the daily power profiles in typical summer and winter days are depicted in Figure 3.

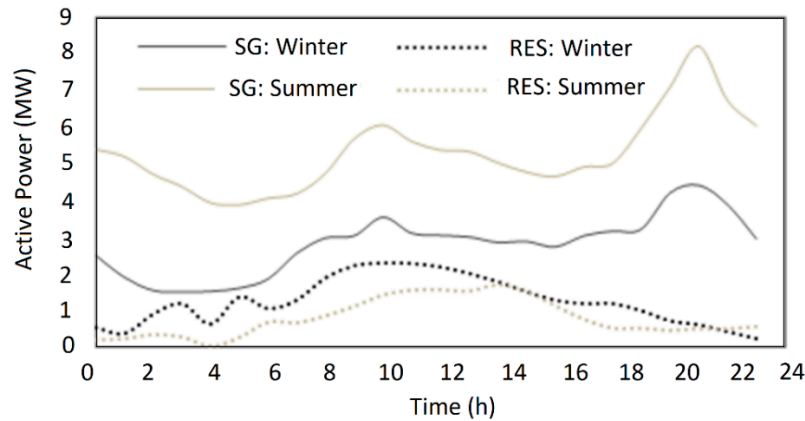


Figure 3. Daily generating profile of SGs and RESs in Pantelleria.

In particular, the dashed line is the daily power profile generated by the VSC, which represents the energy mix composed of wind and photovoltaic plants. According to the power profiles in Figure 3, the inertia  $T_S$  of the isolated power system in each instant is evaluated as follows [26]:

$$T_S = \frac{\sum_1^{N_g} T_i \cdot A_{n,i}}{P_{load}} \tag{13}$$

where  $T_i$  is the inertia and  $A_{n,i}$  is the rated apparent power of the  $i$ -th synchronous generator connected to the grid, and  $P_{load}$  is the total active power requested by the load at each instant.

The worst case, defined as the working condition presenting the least inertia, is defined in Table 4 for both summer (scenario A) and winter (scenario B).

Table 4. Parameters for the considered case study.

Description	Summer	Winter
$T_{SG}$ (s)	1.01	1.29
$T_S$ (s)	0.77	0.45
NSPL	24%	65%
$P_{load}$ (MVA)	6.08	3.56
Hour	9	11

In Table 4, NSPL refers to the non-synchronous penetration level. VSPL can be defined as the rate between the total power generated by RESs and the total power generated at a given hour [27]. The load at the PCC is modelled as a fixed impedance, where the real power  $P_{load}$  and the reactive power  $Q_{load}$  are evaluated as follows:

$$P_{load} = P_{load-0} \cdot \left(\frac{V_{base}}{V_n}\right)^{NP} \cdot (1 + K_{PF} \cdot \Delta F) \tag{14}$$

$$Q_{load} = Q_{load-0} \cdot \left(\frac{V_{base}}{V_n}\right)^{NQ} \cdot (1 + K_{QF} \cdot \Delta F) \tag{15}$$

where  $\Delta$  is the frequency variation;  $V_n$  is the rated voltage,  $P_{load-0}$  and  $Q_{load-0}$  are the active and reactive power of the load at the rated voltage and frequency, respectively; and  $NP$ ,  $K_{PF}$ ,  $NQ$ , and  $K_{QF}$  are the indexes expressing the dependence of active and reactive power from the actual values of the voltage and frequency [20].

The grid has been simulated in the case of a phase-to-phase fault. The flowchart in Figure 4 represents the methodology of the proposed control strategy. The proposed methodology has the ability to deal with fault conditions and to check the VSM behavior in normal and fault operations.

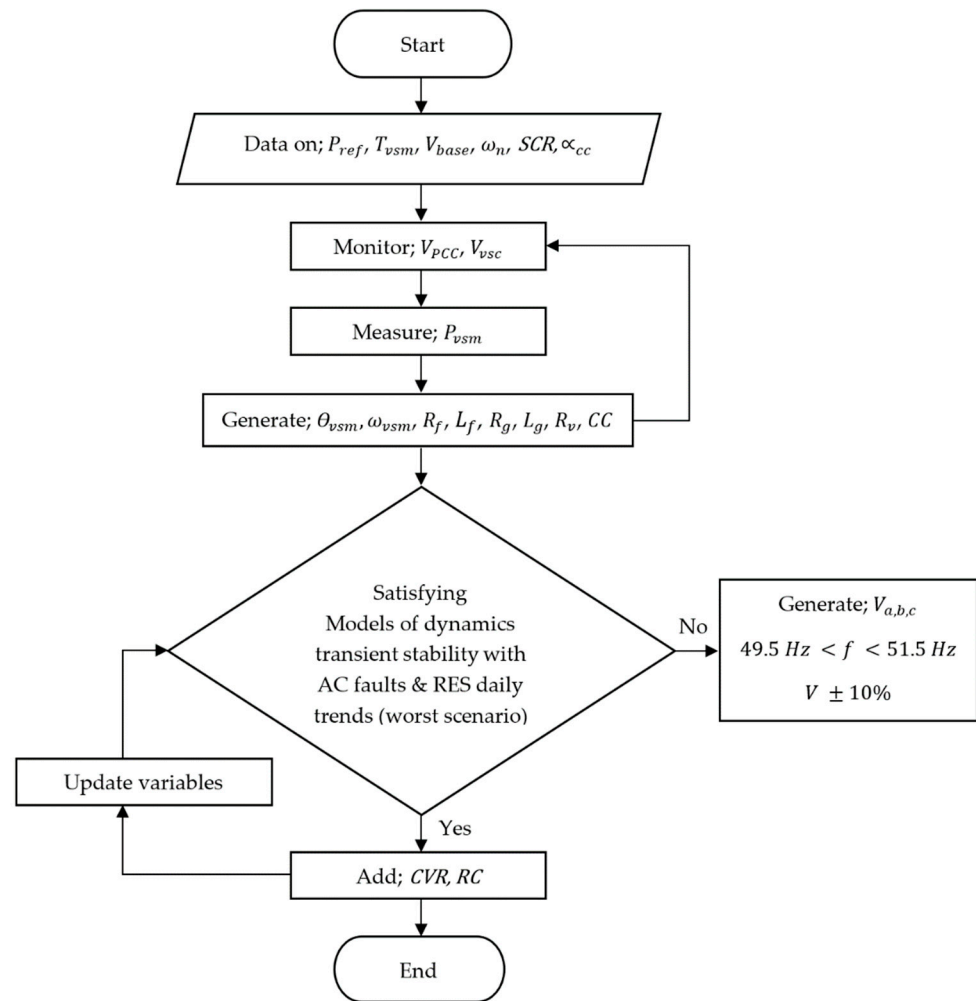


Figure 4. Flow chart of the proposed control strategy.

#### 4. Results and Discussion

In the simulations, the following parameters were considered:  $\zeta = 0.707$ ;  $\omega_n = 10$ ;  $\alpha_{cc} < 0.1 \cdot 2 \cdot \pi \cdot f_s$ ;  $f_s = 5$  kHz. The system was simulated for two different  $T_{vsm}$  values equal to 8 s and 0.01 s.

Four scenarios were considered: two for winter and two for summer.

For sake of simplicity, the scenarios were indicated as A1, A2, B1, and B2, where A was used for winter, B for summer, 1 for option I of RC, and 2 for option II of RC.

The system was tested in the presence of a double-phase fault applied at  $t = 45$  s. To investigate the performance of the VSM control in two extreme fault conditions, two different values of the short-circuit resistance  $R_{sc}$  were considered:  $0.5 \Omega$  and  $0.5 \text{ k}\Omega$ .

Moreover, with the aim to allow for compensating for the delay introduced by PWM using synchronous sampling [20], VCC was examined by considering two angle options for the dq-frame transformation:

1.  $\theta_{vsm}$ ;
2.  $\theta_{comp} = \theta_{vsm} + \theta_0$ , where  $\theta_0 = 1.5\omega_0 / \alpha_{cc}$ .

Finally, two values of SCR were considered:  $SCR = 10$  and  $SCR = 3$ , representing the hypotheses of a strong and weak grid, respectively.

##### 4.1. Strong Grid: $SCR = 10$

The trends of the active power obtained in the simulation for this case are reported in Appendix A Figure A1. The main results of the simulations are summarized below:

- Throughout all of the simulations, a typical trend in grid stability was observed after the fault, with a loss of load, depending on the unbalance between SG and RES. However, because of the action of the speed regulators on the SG and of the internal controllers of the VSC, the active power returned to the previous steady-state values as soon as the fault was removed.
- When the contribution of RES was greater than 60% of the load (Scenarios B1 and B2), and when  $R_{sc}$  assumed its lowest value, the active power showed more significant oscillations. On the other hand, the grid stability improved when angle compensation was used and  $T_{vsm}$  was raised.
- In Scenario A1, the system had a positive behavior; this feature was due to the contribution of both SG and the control option chosen for the VSC (RC-1) during the fault. These choices ensured that scenario A1 did not present unstable situations even in the case of a low  $T_{vsm}$  and  $R_{sc}$ .
- In Scenario A2 with a low value of  $R_{sc}$ , the system became unstable when RC-2 was chosen, regardless the value of  $T_{vsm}$ .
- In the steady-state operation, RC-2 showed a better performance than RC-1, and when using this control option, the system stabilized quickly, as shown in the results for scenarios A2 and B2. However, in the presence of faults, this control option was not able to maintain the desired power.

#### 4.2. Weak Grid: SCR = 3

The successful cases obtained for the strong grid (case with option RC-1) were also examined for the case of a weak grid. The trends of the active power obtained in the simulation for this case are reported in Appendix A Figure A2. The main results of the simulations are summarized below:

- In Scenario A1, no alterations were seen in the power generation from the SG: traditional generators delivered the desired power to the load. On the other hand, in Scenario B1, the power production was reduced to 66% and this created a deficit in power generation.
  - The lower the SCR (and so, the higher the grid reactance,  $X_g$ ), the closer the power contribution of VSC to that of SG. Mathematically, this could be seen by calculating the  $SCR = S_{sc}/S$ , where  $S$  is the VSC rated power and  $S_{sc} = V^2/X_g$  is the grid short-circuit power;
  - The behavior of VSC during the fault did not vary.
- The PCC voltage was significantly affected by the SCR value, as shown in Figure 5, where:
- the voltage variation during the fault was shown for both the robust and the weak grid;
  - there was a variation in the PCC voltage when the power system operated at different transfer power conditions;
  - Scenario A1 was less affected by the SCR value;
  - Scenario B1 with SCR = 3 did not meet the minimum standard established for the voltage value.

Finally, a harmonic analysis of the PCC voltage until the 15th harmonic was carried out, as shown in Figure 6. The dominant harmonic components were found to be the 2nd to the 4th. Figure 6 shows that correct sizing of the VSC filter permitted maintaining an acceptable level of grid power quality. The THD of the PCC voltage did not exceed the limit of 1%. The results of the simulations in Scenario B1 showed the 2nd, 3rd, 10th and 15th harmonics were more or less triple with respect to Scenario A1, and the harmonics from the 4th to the 9th were double.

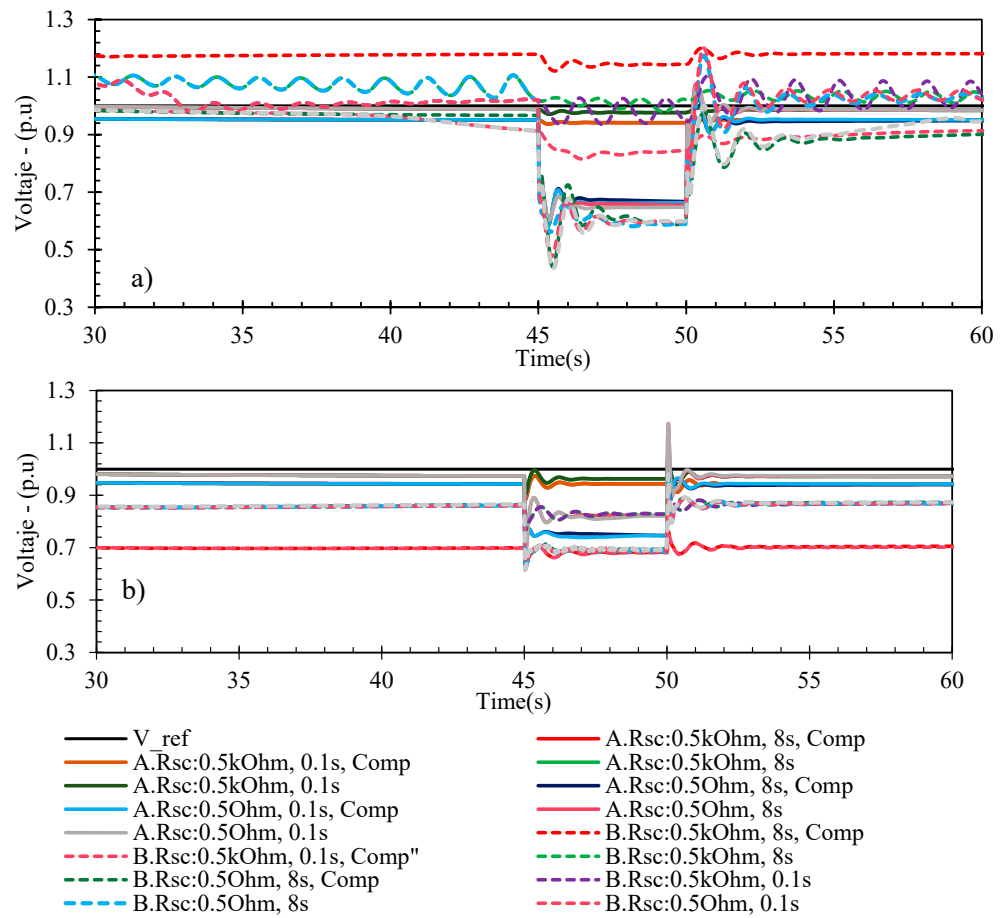


Figure 5. PCC voltage for cases A1 and B1 where (a) represents SCR = 10 and (b) represents SCR = 3.

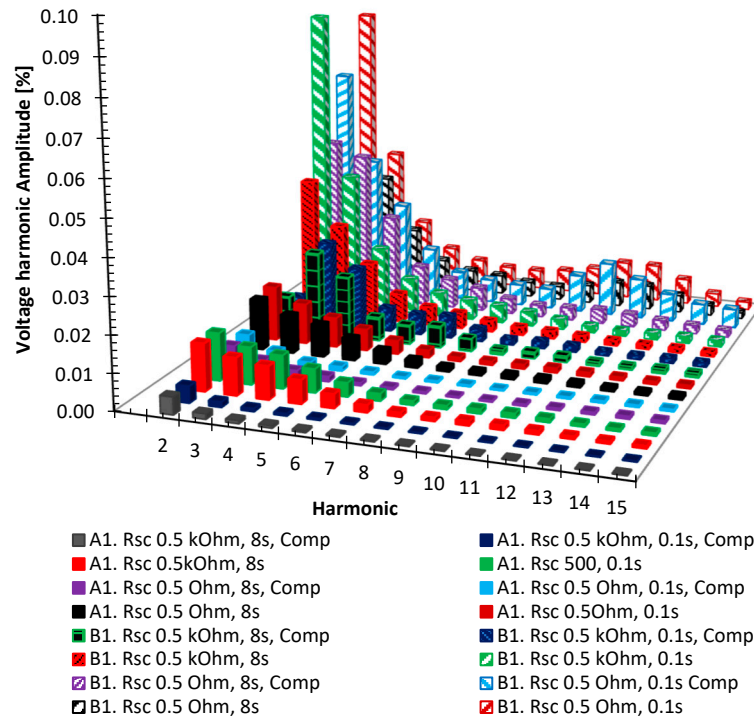


Figure 6. PCC voltage harmonic spectrum.

## 5. Conclusions

Using VSC with a swing controller and VCC with two different options for the RC on RES-based generators has been demonstrated to have mutual advantages in normal and faulty operation for small isolated power systems. The proposed VSM model allows for the implementation of virtual inertia and damping in the isolated grid, also improving grid stability in the presence of extremely severe fault situations such as those represented by the phase-to-phase fault. In the simulations performed for the Island of Pantelleria in the Mediterranean Sea, the transients of the active power output of the VSC and of the voltage at the PCC have been observed. The study shows how the value of the SCR can influence the behavior of the VSC. Moreover, the acceptable level of grid power quality has been ensured via harmonic analysis of the PCC voltage. The precise design of different stages of the proposed model is required to maximize the benefits gained in both the static and dynamic behavior of the isolated grids.

The performed study is useful for setting the parameters of the VSM control of VSCs in small islands not supplied by the main power transmission grid; however, this is only a first step of a more complex process for fostering the penetration of RESs in small islands.

Indeed, some other aspects must be considered before transformation towards a 100% RES-based generation system can be achieved. For example, there is still a lack of research in the determination of the required amount of power from VSC with VSM control that can be installed without creating a stability issue in the grid due to the interactions between converters. This study has been already started and is partially presented in [11], and will be the next important step in the current research on VSM application to small island power systems.

**Author Contributions:** Conceptualization, M.A.N.N. and G.Z.; methodology, S.F.; validation, G.Z. and J.A.S.; formal analysis, J.A.S. and M.A.N.N.; writing—original draft preparation, M.A.N.N. and G.Z.; writing—review and editing, J.A.S. and S.F.; supervision, S.F. All authors have read and agreed to the published version of the manuscript.

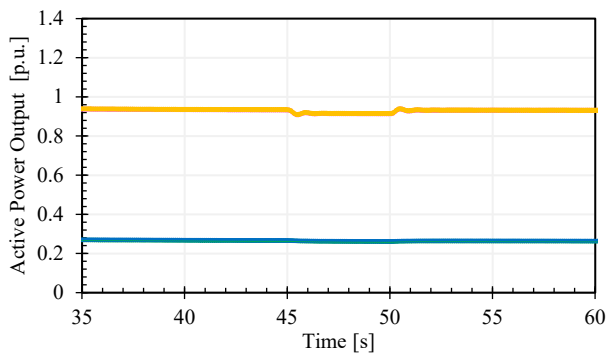
**Funding:** This research received no external funding.

**Acknowledgments:** The present work was realized in the framework of the Research Cooperation Agreement between the Engineering Department of the University of Palermo and the Department of Electrical and Computer Engineering of Birzeit University, for the project DGWG (Distributed Generation integration in Weak Grids).

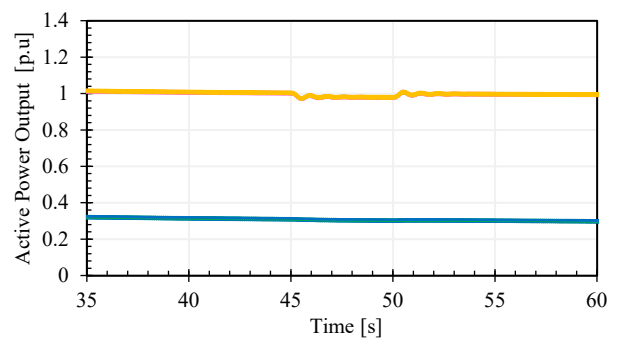
**Conflicts of Interest:** The authors declare no conflict of interest.

## Appendix A

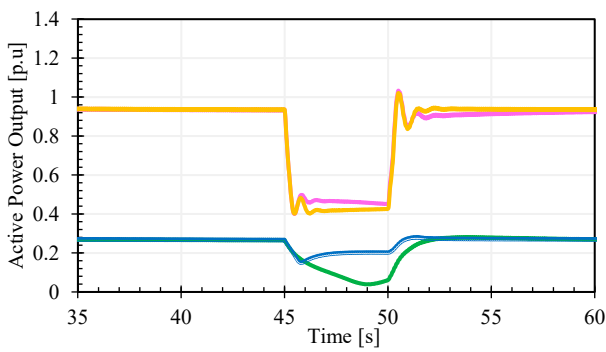
The graphs of Figure A1 represent the load and RES active power in the case of a strong grid (SCR = 10).



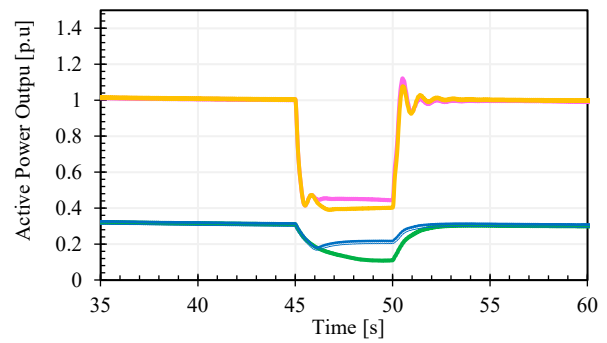
(a) Scenario A1,  $\theta = \theta_{comp}$ ;  $R_{sc} = 0.5 \text{ k}\Omega$ ;



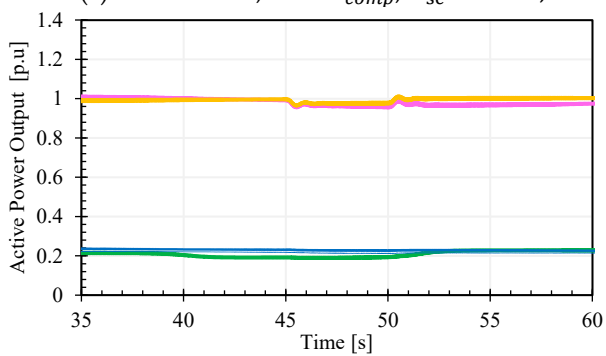
(b) Scenario A1,  $\theta = \theta_{vsmi}$ ;  $R_{sc} = 0.5 \text{ k}\Omega$ ;



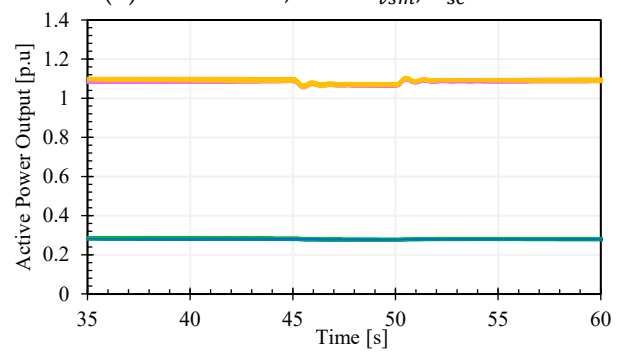
(c) Scenario A1,  $\theta = \theta_{comp}$ ;  $R_{sc} = 0.5 \Omega$ ;



(d) Scenario A1,  $\theta = \theta_{vsmi}$ ;  $R_{sc} = 0.5 \Omega$

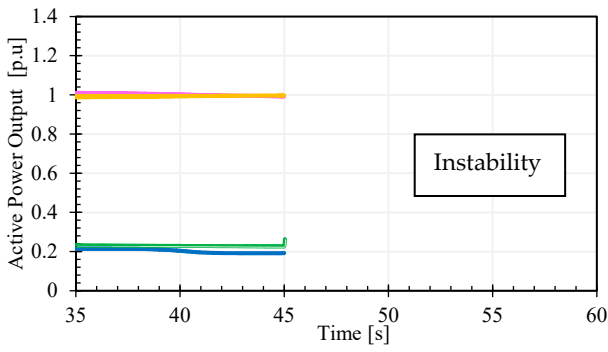


(e) Scenario A2,  $\theta = \theta_{comp}$ ;  $R_{sc} = 0.5 \text{ k}\Omega$ ;

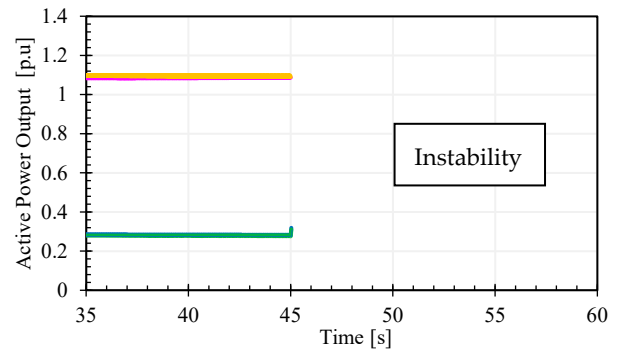


(f) Scenario A2,  $\theta = \theta_{vsmi}$ ;  $R_{sc} = 0.5 \text{ k}\Omega$ ;

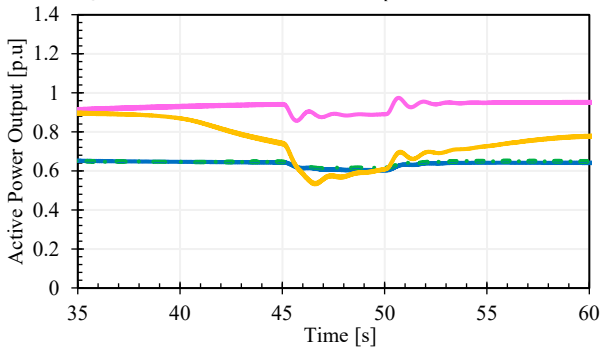
Figure A1. Cont.



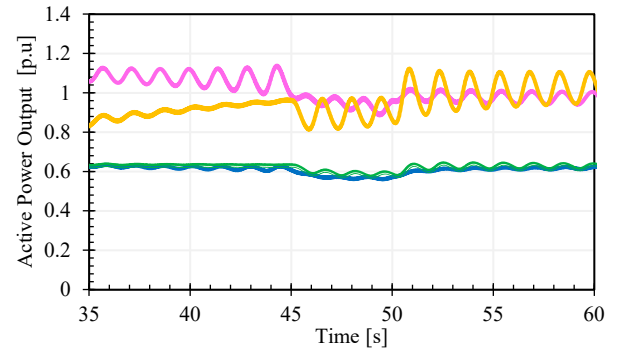
(g) Scenario A2,  $\theta = \theta_{comp}$ ;  $R_{sc} = 0.5 \Omega$ ;



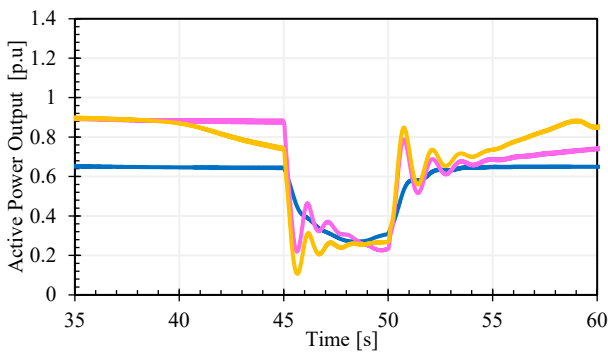
(h) Scenario A2,  $\theta = \theta_{vsm}$ ;  $R_{sc} = 0.5 \Omega$



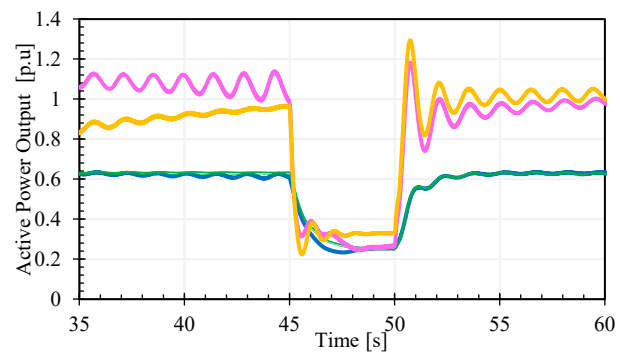
(i) Scenario B1,  $\theta = \theta_{comp}$ ;  $R_{sc} = 0.5 \text{ k}\Omega$ ;



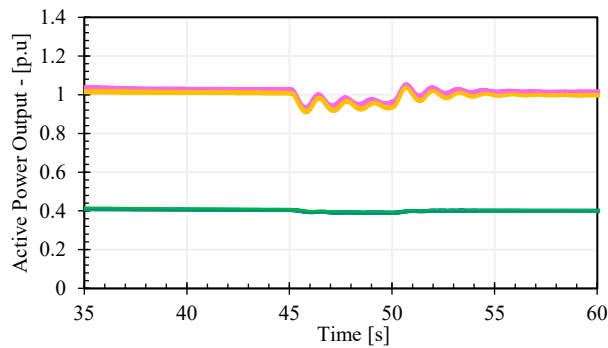
(j) Scenario B1,  $\theta = \theta_{vsm}$ ;  $R_{sc} = 0.5 \text{ k}\Omega$ ;



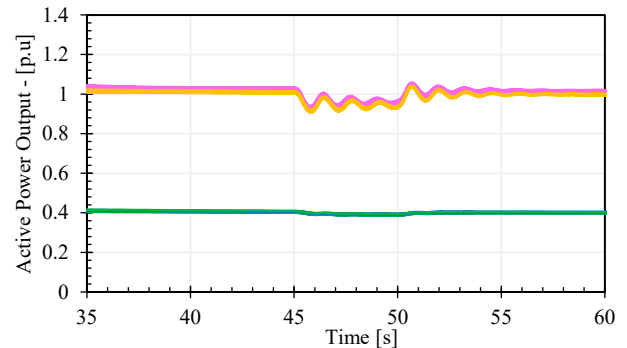
(k) Scenario B1,  $\theta = \theta_{comp}$ ;  $R_{sc} = 0.5 \Omega$ ;



(l) Scenario B1,  $\theta = \theta_{vsm}$ ;  $R_{sc} = 0.5 \Omega$

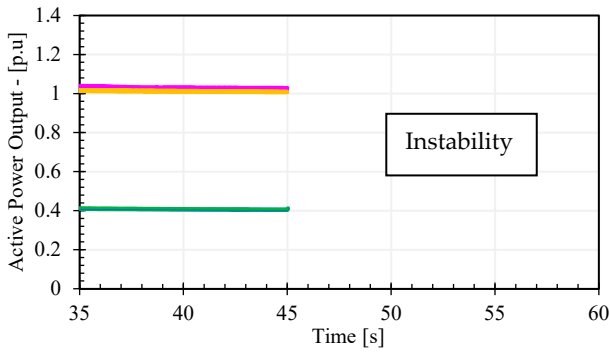


(m) Scenario B2,  $\theta = \theta_{comp}$ ;  $R_{sc} = 0.5 \text{ k}\Omega$ ;

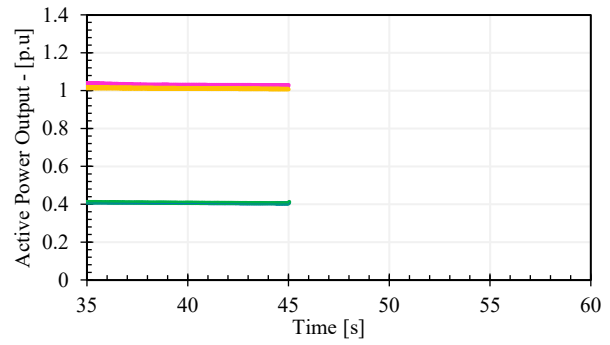


(n) Scenario B2,  $\theta = \theta_{vsm}$ ;  $R_{sc} = 0.5 \text{ k}\Omega$ ;

Figure A1. Cont.



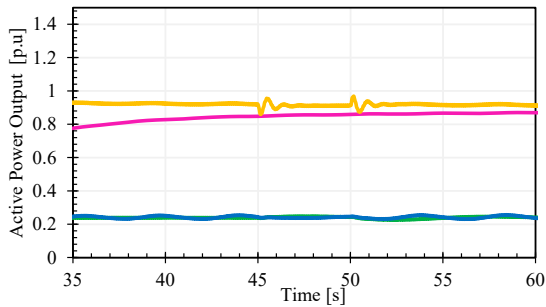
(o) Scenario B2,  $\theta = \theta_{comp}$ ;  $R_{sc} = 0.5 \Omega$ ;



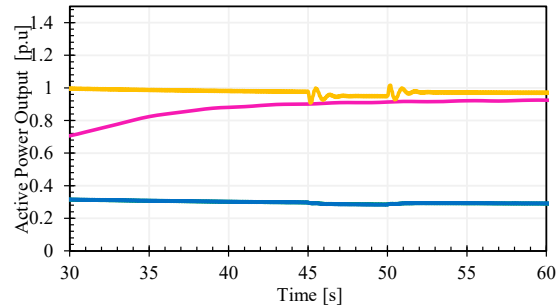
(p) Scenario B2,  $\theta = \theta_{vsmi}$ ;  $R_{sc} = 0.5 \Omega$

**Figure A1.** Load and RES active power with SCR = 10.

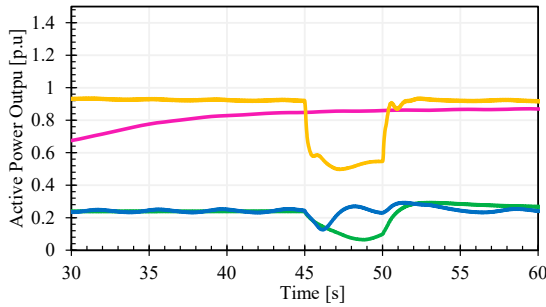
The graphs in Figure A2 represent the load and RES active power in the case of a weak grid (SCR = 3).



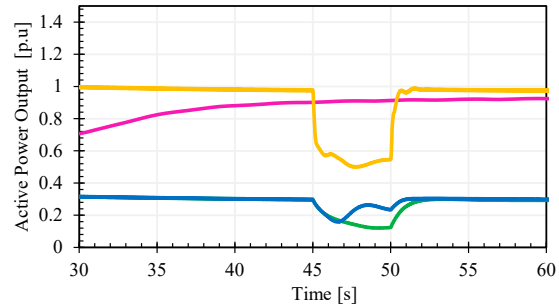
(a) Scenario A1,  $\theta = \theta_{comp}$ ;  $R_{sc} = 0.5 \text{ k}\Omega$ ;



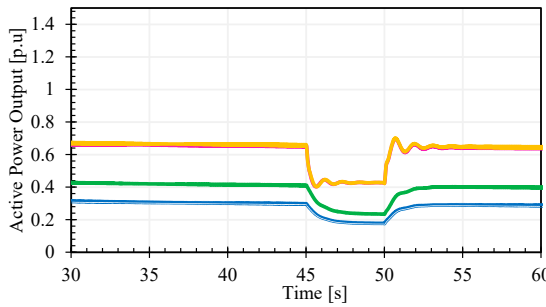
(b) Scenario A1,  $\theta = \theta_{vsmi}$ ;  $R_{sc} = 0.5 \text{ k}\Omega$ ;



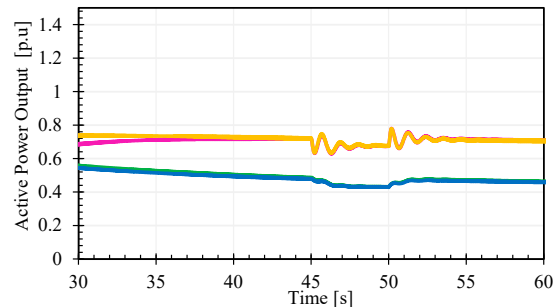
(c) Scenario A1,  $\theta = \theta_{comp}$ ;  $R_{sc} = 0.5 \Omega$ ;



(d) Scenario A1,  $\theta = \theta_{vsmi}$ ;  $R_{sc} = 0.5 \Omega$



(e) Scenario B1,  $\theta = \theta_{comp}$ ;  $R_{sc} = 0.5 \text{ k}\Omega$ ;



(f) Scenario B1,  $\theta = \theta_{vsmi}$ ;  $R_{sc} = 0.5 \text{ k}\Omega$ ;

**Figure A2.** Cont.

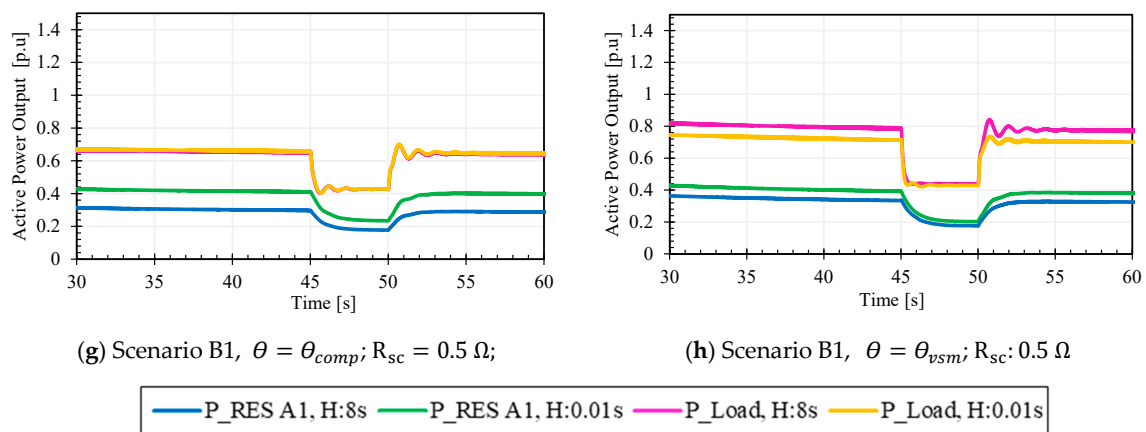


Figure A2. Load and RES active power with SCR = 3.

## References

- Campocchia, A.; Dusonchet, L.; Telaretti, E.; Zizzo, G. Financial measures for supporting wind power systems in Europe: A comparison between green tags and feed in tariffs. In Proceedings of the International Symposium on Power Electronics, Electrical Drives, Automation and Motion, Ischia, Italy, 11–13 June 2008.
- Sa'Ed, J.A.; Amer, M.; Bodair, A.; Baransi, A.; Favuzza, S.; Zizzo, G. A Simplified Analytical Approach for Optimal Planning of Distributed Generation in Electrical Distribution Networks. *Appl. Sci.* **2019**, *9*, 5446. [[CrossRef](#)]
- Ippolito, M.G.; Musca, R.; Zizzo, G. Frequency dynamics of power systems with temporally distributed disturbances. *Sustain. Energy Grids Netw.* **2021**, *28*, 100536. [[CrossRef](#)]
- Papakonstantinou, A.G.; Papathanassiou, S.A. Battery Energy Storage Participation in Automatic Generation Control of Island Systems, Coordinated with State of Charge Regulation. *Appl. Sci.* **2022**, *12*, 596. [[CrossRef](#)]
- Cheema, K.M.; Chaudhary, N.I.; Tahir, M.F.; Mehmood, K.; Mudassir, M.; Kamran, M.; Milyani, A.H.; Elbarbary, Z.M.S. Virtual synchronous generator: Modifications, stability assessment and future applications. *Energy Rep.* **2022**, *8*, 1704–1717. [[CrossRef](#)]
- Muftau, B.; Fazeli, M. The Role of Virtual Synchronous Machines in Future Power Systems: A Review and Future Trends. *Electr. Power Syst. Res.* **2022**, *206*, 107775. [[CrossRef](#)]
- Cheema, K.M. A comprehensive review of virtual synchronous generator. *Int. J. Electr. Power Energy Syst.* **2020**, *120*, 106006. [[CrossRef](#)]
- Tamrakar, U.; Shrestha, D.; Maharjan, M.; Bhattarai, B.P.; Hansen, T.M.; Tonkoski, R. Virtual Inertia: Current Trends and Future Directions. *Appl. Sci.* **2017**, *7*, 654. [[CrossRef](#)]
- Liu, C.; Fang, J. Analysis and Design of Inertia for Grid-Tied Electric Vehicle Chargers Operating as Virtual Synchronous Machines. *Appl. Sci.* **2022**, *12*, 2194. [[CrossRef](#)]
- Leng, D.; Polmai, S. Virtual Synchronous Generator Based on Hybrid Energy Storage System for PV Power Fluctuation Mitigation. *Appl. Sci.* **2019**, *9*, 5099. [[CrossRef](#)]
- Ippolito, M.G.; Musca, R.; Sanseverino, E.R.; Zizzo, G. Frequency Dynamics in Fully Non-Synchronous Electrical Grids: A Case Study of an Existing Island. *Energies* **2022**, *15*, 2220. [[CrossRef](#)]
- Corso, G.; Di Silvestre, M.L.; Ippolito, M.G.; Sanseverino, E.R.; Zizzo, G. Multi-objective long term optimal dispatch of distributed energy resources in micro-grids. In Proceedings of the 45th International Universities' Power Engineering Conference—UPEC 2010, Cardiff, UK, 31 August–3 September 2010.
- Ippolito, M.G.; Musca, R.; Zizzo, G.; Bongiorno, M. Damping Provision by Different Virtual Synchronous Machine Schemes. In Proceedings of the IEEE International Conference on Environment and Electrical Engineering and IEEE Industrial and Commercial Power Systems Europe—EEEIC/I&CPS Europe, Madrid, Spain, 16–18 June 2020.
- Ippolito, M.G.; Musca, R.; Zizzo, G.; Bongiorno, M. Extension and Tuning of Virtual Synchronous Machine to Avoid Oscillatory Instability in Isolated Power Networks. In Proceedings of the AEIT International Annual Conference—AEIT, Bari, Italy, 23–25 September 2020.
- Sa'ed, J.A.; Curto, D.; Favuzza, S.; Musca, R.; Navia, M.N.; Zizzo, G.A. Simulation Analysis of VSM Control for RES plants in a Small Mediterranean Island. In Proceedings of the IEEE International Conference on Environment and Electrical Engineering and IEEE Industrial and Commercial Power Systems Europe—EEEIC/I&CPS Europe, Madrid, Spain, 16–18 June 2020.
- Favuzza, S.; Ippolito, M.G.; Navarro, M.; Sanseverino, E.R.; Zizzo, G.; Bongiorno, M. An Analysis of the Inertial Response of Small Isolated Power Systems in Presence of Generation from Renewable Energy Sources. In Proceedings of the IEEE 4th International Forum on Research and Technology for Society and Industry—RTSI, Palermo, Italy, 10–13 September 2018.
- Bongiorno, M.; Favuzza, S.; Ippolito, M.G.; Musca, R.; Zizzo, G. Inertial Response of Isolated Power Networks with Wind Power Plants. In Proceedings of the IEEE PowerTech, Milan, Italy, 23–27 June 2019.

18. Favuzza, S.; Ippolito, M.G.; Musca, R.; Navia, M.N.; Sanseverino, E.R.; Zizzo, G.; Bongiorno, M. System Stability of a Small Island's Network with Different Levels of Wind Power Penetration. In Proceedings of the IEEE 4th International Forum on Research and Technology for Society and Industry—RTSI, Palermo, Italy, 10–13 September 2018.
19. D'Arco, S.; Suul, J.A.; Fosso, O.B. A Virtual Synchronous Machine implementation for distributed control of power converters in SmartGrids. *Electr. Power Syst. Res.* **2015**, *122*, 180–197. [[CrossRef](#)]
20. Blaabjerg, F.; Teodorescu, R.; Liserre, M.; Timbus, A.V. Overview of Control and Grid Synchronization for Distributed Power Generation Systems. *IEEE Trans. Ind. Electron.* **2006**, *53*, 1398–1409. [[CrossRef](#)]
21. Guan, M.; Pan, W.; Zhang, J.; Hao, Q.; Cheng, J.; Zheng, X. Synchronous Generator Emulation Control Strategy for Voltage Source Converter (VSC) Stations. *IEEE Trans. Power Syst.* **2015**, *30*, 3093–3101. [[CrossRef](#)]
22. Rodriguez, P.; Timbus, A.V.; Teodorescu, R.; Liserre, M.; Blaabjerg, F. Flexible Active Power Control of Distributed Power Generation Systems During Grid Faults. *IEEE Trans. Ind. Electron.* **2007**, *54*, 2583–2592. [[CrossRef](#)]
23. Beza, M. Power System Stability Enhancement Using Shunt-connected Power Electronic Devices with Active Power Injection Capability. Ph.D. Thesis, Chalmers University of Technology, Gothenburg, Sweden, 2015.
24. Crainz, M.; Curto, D.; Franzitta, V.; Longo, S.; Montana, F.; Musca, R.; Sanseverino, E.R.; Telaretti, E. Flexibility Services to Minimize the Electricity Production from Fossil Fuels. A Case Study in a Mediterranean Small Island. *Energies* **2019**, *12*, 3492. [[CrossRef](#)]
25. Massaro, F.; Pace, G.; Sanseverino, E.R.; Tanaka, K.; Zizzo, G. An Algorithm for Optimal Sizing of BESS in Smart Island Energy Communities: The Case of Pantelleria. In Proceedings of the IEEE International Conference on Environment and Electrical Engineering and IEEE Industrial and Commercial Power Systems Europe—EEEIC/I&CPS Europe, Bari, Italy, 7–10 September 2021.
26. ENTSO-E Report. Future System Inertia. Available online: [https://eepublicdownloads.entsoe.eu/clean-documents/Publications/SOC/Nordic/Nordic\\_report\\_Future\\_System\\_Inertia.pdf](https://eepublicdownloads.entsoe.eu/clean-documents/Publications/SOC/Nordic/Nordic_report_Future_System_Inertia.pdf) (accessed on 1 March 2022).
27. Curto, D.; Favuzza, S.; Franzitta, V.; Musca, R.; Navia, M.A.N.; Zizzo, G. Evaluation of the optimal renewable electricity mix for Lampedusa island: The adoption of a technical and economical methodology. *J. Clean. Prod.* **2020**, *263*, 121404. [[CrossRef](#)]